Earth and Planetary Science Letters 498 (2018) 334–347

Contents lists available at ScienceDirect

Earth and Planetary Science Letters

www.elsevier.com/locate/epsl

Seismicity and structure of Nazca Plate subduction zone in southern Peru

Hobin Lim [a], YoungHee Kim [a,*], Robert W. Clayton [b], Clifford H. Thurber [c]

[a] School of Earth and Environmental Sciences, Seoul National University, Seoul, 08826, Republic of Korea
[b] Division of Geological and Planetary Sciences, California Institute of Technology, Pasadena, CA 91125, USA
[c] Department of Geoscience, University of Wisconsin-Madison, Madison, WI 53706-1692, USA

ARTICLE INFO

Article history:
Received 31 January 2018
Received in revised form 5 July 2018
Accepted 10 July 2018
Available online 20 July 2018
Editor: M. Ishii

Keywords:
seismicity
subduction zone system
Nazca Plate
relocation
double-difference tomography
southern Peru

ABSTRACT

We define subducting plate geometries in the Nazca subduction zone by (re)locating intra-slab earthquakes in southern Peru (14–18°S) and using previously published converted phase analysis results to clarify the slab geometry and inferred relationships to the seismicity. We also provide both *P*- and *S*-wave velocity models of the subducting Nazca Plate and mantle layer above the slab using double-difference tomography to understand upper-plate volcanism and subduction zone process. The double-difference constraints for determining the hypocenters and velocity model ensure high accuracy of the relative location of earthquakes with respect to velocity structure. The relocated seismicity shows a smooth contortion in the slab-dip transition zone for ~400 km between the shallow (30°)-to-flat dipping interface to the northwest and the 30°-dipping interface to the southeast. We find a significant slab-dip difference (up to 10°) between our results and previous slab models along the profile region sampling the horizontal slab at a depth of ~85–95 km. Robust features in both *P*- and *S*-wave tomography inversions are both arc-normal and along-arc velocity variations. In the arc-normal direction, all profile results show that the slab velocities beneath the forearc (down to a depth of ~100 km) transition to higher velocities beneath the backarc (at ~100–140 km depth). In the along-arc direction, velocities of the subducting flat slab are shown to be depressed compared to those of the normal-dip slab. In addition, high shear-wave velocities and low *Vp*/*Vs* are detected in the mantle layer above the flat slab, indicating its cold and dry environment. Such differences in the velocity structures for the slab and mantle wedge between the two regions may indicate different hydration states, which greatly affects the upper-plate structure of southern Peru.

1. Introduction

Along the South American margin between 2°S and 20°S latitude, the Nazca Plate subducts beneath the South American Plate, causing earthquakes, volcanism and upper-plate deformation. Earthquakes in this region exhibit complex rupture characteristics that are related to subducting asperities on the Nazca Plate (Bilek, 2010). In particular, significant subduction-zone complexity in S. Peru has been previously attributed to the moderate-size (~200 km × 18 km) Nazca Ridge and the Nazca fracture zone (Fig. 1). This region includes a transition in slab geometry from flat to normal from north to south (Cahill and Isacks, 1992; Hayes et al., 2012; Phillips et al., 2012; Phillips and Clayton, 2014; Kim et al., 2015; Ma and Clayton, 2015; Bishop et al., 2017), decrease in magmatic activity towards the flat slab subduction (Ramos and Folguera, 2009), and variability in earthquake rupture patterns and coupling state (Chlieh et al., 2011). The flat slab system developed at 11.2 Ma when the buoyant ridge collided with the forearc at ~11°S, and since that time the ridge has been migrating southward (Hampel, 2002). Its present location coincides with the southern end of the flat subduction segment, where the dense seismic arrays are available. In this study, we exploit array data from the Peru Subduction Experiment (PeruSE, 2013) and the Central Andes Uplift and Geophysics of High Topography (CAUGHT; Beck et al., 2010) experiment to better define the subduction zone geometry and constrain the plate boundary dynamics in the slab-dip transition zone at 14–18°S latitude and at 30–130-km depth (Fig. 1).

Earthquake locations typically provide a first-order estimate of the slab geometry, and by exploiting the relatively long South American earthquake catalog, various groups have constructed

* Corresponding author.
E-mail addresses: hbim7676@snu.ac.kr (H. Lim), younghkim@snu.ac.kr (Y. Kim), clay@gps.caltech.edu (R.W. Clayton), cthurber@wisc.edu (C.H. Thurber).

https://doi.org/10.1016/j.epsl.2018.07.014
0012-821X/

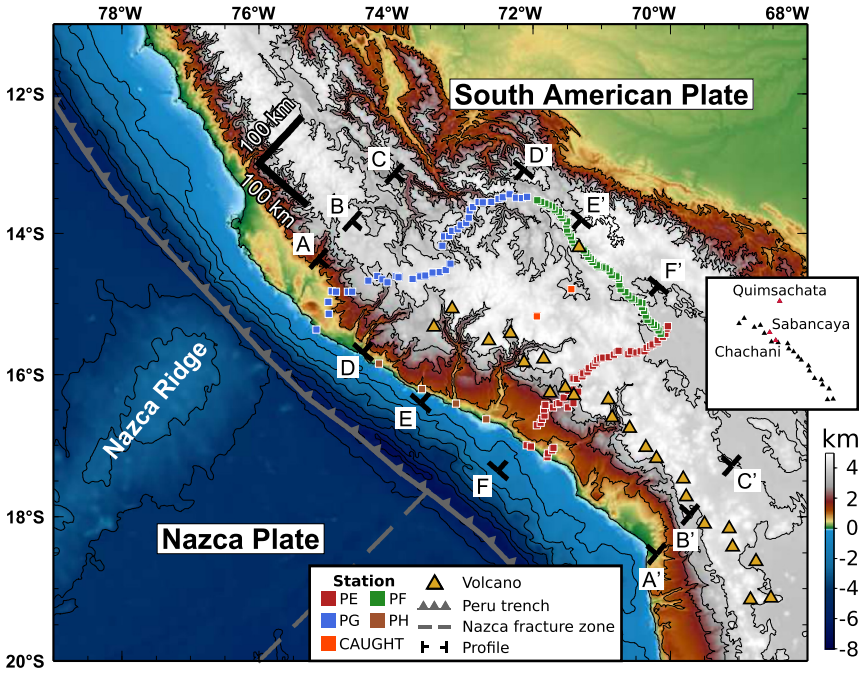

Fig. 1. Topographic–bathymetric map of the study region. Seismic data used in this study are from Peru Subduction Experiment (PeruSE, 2013) and Central Andes Uplift and Geophysics of High Topography (CAUGHT). The topography and bathymetry are contoured with 1000 m interval. Inset indicates the locations of volcanos Quimsachata, Sabancaya, and Chachani. (For interpretation of the colors in the figure(s), the reader is referred to the web version of this article.)

slab geometry models defined by earthquake locations determined from regional and teleseismic recordings (Figs. 2, 3 and S1–3). The sparsity of the regional seismic network, however, results in a significant disagreement among these models, particularly in the iso-depth contour lines of the Nazca slab at 50 and 100 km, which show the least coherence (Figs. 2, 3 and S1–3). Furthermore, the correlation between the location of the volcanic front and the corresponding slab depth is neither clear nor consistent among the models (Figs. 2, 3 and S1–3). The location of the plate interface beneath the stations is most directly resolved using methods based on teleseismic *P*-to-*S* converted phases (Phillips et al., 2012; Phillips and Clayton, 2014; Kim and Clayton, 2015; Ma and Clayton, 2015; Bishop et al., 2017). However, these types of analyses do not constrain the plate geometry between the two linear arrays (PE and PG; Fig. 1) in the region where the horizontally subducting Nazca slab transitions into a normal-dipping slab.

In this study, we focus on the region of flat-slab subduction where the Nazca Ridge subducts; the normal-dip subduction zone south of Nazca Ridge; and most importantly, the region between the two to examine along-strike variations in plate geometry and seismic velocities at depths of 30–130 km. We use regional earthquakes recorded from PeruSE, which consists of three dense seismic array lines surrounding the region between the flat and normal Nazca slab systems and four stations deployed along the coast, and two stations from the CAUGHT network (Fig. 1). Using images based on the relocated seismicity and double-difference tomography (Zhang and Thurber, 2003), we clarify the Nazca Plate geometry and inferred relationships to the subduction process, volcanism in the upper plate, and the occurrence of earthquakes.

2. Data and methods

2.1. Data and initial velocity model

We use the data recorded from the temporary seismic arrays in S. Peru (142 stations from PeruSE and 2 from CAUGHT) from July 2008 to April 2013 (Fig. 1). Interstation spacing of PeruSE is 6–10 km for the PE, PG and PF lines and ∼75 km for the PH line (Fig. 1). We detect local earthquakes using FilterPicker, an automatic picking program that uses multiple frequency bands (Lomax et al., 2012). The program generates over 34 million picks, of which we select only those in which the difference in trigger times is less than the interstation distances divided by the apparent *P*-wave velocity of 7.0 km/s. Of the 451 earthquakes selected within the study region (Table S1), we manually pick the *P* wave on vertical-component data and the *S* on the transverse-component data. The *S* phase effectively reduces a trade-off between origin time and the depth of intermediate-depth (>100 km) hypocenters.

Initial hypocenters are determined by inverting the arrival times of the *P* and *S* phases and using the AK135 velocity model (Kennett et al., 1995) as an initial model. These arrival times are also used to obtain 1-D and 3-D velocity models of the region (see the Supplementary Material). Figs. S4a and b and Table S2 show the optimal 1-D model derived in this study. The hypocenters are then determined based on Markov Chains Monte Carlo method (Myers et al., 2007).

2.2. Double-difference tomography

We apply the double-difference tomography method (Zhang and Thurber, 2003), which jointly inverts, for earthquake hypocenters, *P*-wave velocity (*Vp*) and *S*-wave velocity (*Vs*). The method minimizes residuals between the observed and calculated arrival times, and the differences between pairs of nearby earthquakes, employing an iterative damped-least-squares method. This method builds on the earthquake location procedure of Waldhauser and Ellsworth (2000), which utilizes the differential times of the *P* and *S* phases. 6559 *P*- and 4145 *S*-wave arrival times are used in the inversion, and 24,212 differential times measured using waveform cross-correlation are used to constrain the relative locations of the events. Nodes for the inversion are spaced 20 km apart laterally and placed on both the arc-normal trench-perpendicular and along-arc trench-parallel directions (Figs. S4c and d). The nodes are placed at 0, 30 and 50 km in depth for sampling the continental crust, and every 20 km in depth from 70 to 410 km for the mantle wedge and slab (Figs. S4c and d). We determine and apply smooth-